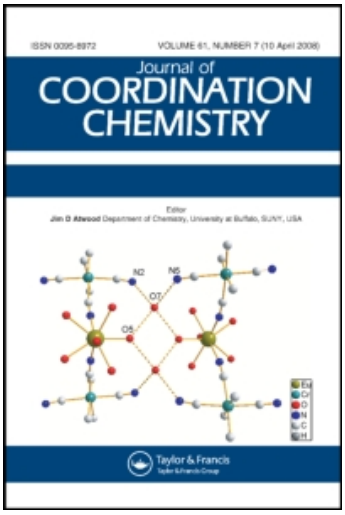

Journal of Coordination Chemistry
Publication details, including instructions for authors and subscription information:
http://www.informaworld.com/smpp/title~content=t713455674

Synthesis, molecular and electronic structure of half-sandwich ruthenium(II) complex with 2-(2-pyridyl)-4-methylthiazole-5-carboxylic acid

J. G. Małecki[a]
[a] Department of Crystallography, Institute of Chemistry, University of Silesia, 40-006 Katowice, Poland

First published on: 15 July 2010

To cite this Article Małecki, J. G.(2010) 'Synthesis, molecular and electronic structure of half-sandwich ruthenium(II) complex with 2-(2-pyridyl)-4-methylthiazole-5-carboxylic acid', Journal of Coordination Chemistry, 63: 13, 2268 — 2277, First published on: 15 July 2010 (iFirst)
To link to this Article: DOI: 10.1080/00958972.2010.502572
URL: http://dx.doi.org/10.1080/00958972.2010.502572

Journal of Coordination Chemistry
Vol. 63, No. 13, 10 July 2010, 2268–2277

Taylor & Francis
Taylor & Francis Group

Synthesis, molecular and electronic structure of half-sandwich ruthenium(II) complex with 2-(2-pyridyl)-4-methylthiazole-5-carboxylic acid

J.G. MAŁECKI*

Department of Crystallography, Institute of Chemistry, University of Silesia, 9th Szkolna St, 40-006 Katowice, Poland

(*Received 7 March 2010; in final form 24 May 2010*)

$[(C_6H_6)RuCl(pmtca)]Cl$ has been prepared and studied by infrared, NMR, UV-Vis spectroscopy, and X-ray crystallography. The complexes were prepared by the reactions of $[(C_6H_6)RuCl_2]_2$ with 2-(2-pyridyl)-4-methylthiazole-5-carboxylic acid in methanol. The electronic structure and UV-Vis spectrum of the obtained compound have been calculated. The electronic structure of the studied complex was calculated using density functional theory. Apart from the descriptions of frontier molecular orbitals and the relocation of the electron density of the compounds, the bonding and π-acceptor properties of the pmtca ligand were also determined.

Keywords: Ruthenium–benzene complexes; 2-(2-Pyridyl)-4-methylthiazole-5-carboxylic acid; X-ray structure; UV-Vis; DFT; TD-DFT

1. Introduction

In the chemistry of ruthenium, complexes containing N-heterocyclic derivatives have wide interest from rich redox chemistry and photophysics. Even small changes in coordination environment around ruthenium play a key role in altering the redox properties of its complexes. Thus, complexation of ruthenium by different ligands has been widely studied [1].

The η^6-arene ruthenium complexes play a vital role in organometallic chemistry [2]. Arene ruthenium halide compounds are key starting materials for the formation of a range of natural and cationic ligand derivatives [3]. The half-sandwich arene ruthenium complexes serve as excellent catalyst precursors for the hydrogenation and ring-opening metathesis polymerization. Recent studies of arene ruthenium complexes have shown that they are found to inhibit cancer cell growth.

The studied compound merges the benefits of half-sandwich ruthenium coordination compounds and complexes containing N,S-heteroaromatic ligands. The article presents the synthesis, crystal, molecular, and electronic structures, and spectroscopic characterization of the new half-sandwich ruthenium(II) complex.

*Email: gmalecki@us.edu.pl

Journal of Coordination Chemistry
ISSN 0095-8972 print/ISSN 1029-0389 online
DOI: 10.1080/00958972.2010.502572

2. Experimental

The starting material $[(C_6H_6)RuCl_2]_2$ was synthesized according to the literature procedure [4]. All other reagents were commercially available and were used without purification.

2.1. *Synthesis*

A mixture of $[(C_6H_6)RuCl_2]_2$ (0.25 g, 5×10^{-4} mol) and 2-(2-pyridyl)-4-methylthiazole-5-carboxylic acid (0.5 g, $\sim 0.7 \times 10^{-4}$ mol) in methanol (50 cm^{-3}) was refluxed for 3 h, cooled, and filtered. Crystals suitable for X-ray crystal analysis were obtained by slow evaporation of the reaction mixture (scheme 1).

1: $[(C_6H_6)RuCl(pmtca)]Cl \cdot 3H_20$ – Yield 87%. IR (KBr): 3650 (ν_{OH}), 3479 (ν_{OH}), 3296, 3069 (ν_{ArH}), 3020 (ν_{CH3}), 1928 ($\nu_{C=O}$), 1697 (ν_{CN}), 1631 ($\nu_{COO\ (as)}$), 1600 (ν_{OH}), 1532 ($\nu_{ring\ pyridil}$), 1483 ($\delta_{C–CH\ in\ the\ plane}$), 1440 ($\delta_{CH3}$), 1251 ($\nu_{COO\ (s)}$), 852 ($\delta_{C–C\ out\ of\ the\ plane}$), 785 ($\nu_{CS}$), 752, 747 ($\delta_{COOH\ out\ of\ the\ plane}$), 439 ($\nu_{Ru–N}$). UV-Vis (methanol, λ [nm] ($\log \varepsilon$)): 440.6 (2.86), 342.1 (3.98), 329.7 (4.15), 216.5 (4.38). ^{1}H NMR: ($CDCl_3$, ppm) 5.613 (s C_6H_6). Anal. Calcd (%) for: C 36.65, H 3.84, Cl 13.52, N 5.34, O 15.26, Ru 19.27, S 6.11. Found (%): C 36.74, N 5.32, H 3.91.

2.2. *Physical measurements*

Infrared (IR) spectra were recorded on a Nicolet Magna 560 spectrophotometer from 4000 to 400 cm^{-1} as KBr pellets. Electronic spectrum was measured on a Lab Alliance UV-Vis 8500 spectrophotometer from 600 to 180 nm in methanol. Elemental analyses (C, H, N) were performed on a Perkin-Elmer CHN-2400 analyzer. The ^{1}H NMR spectrum was obtained at room temperature in $CDCl_3$ using a Bruker 400 spectrometer.

2.3. *DFT calculations*

Calculations were carried out using Gaussian09 [5] program. The DFT/B3LYP [6] method was used for geometry optimization and electronic structure determination, and electronic spectra were calculated by time-dependent-density functional theory

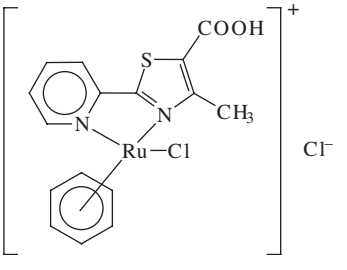

Scheme 1. Structural drawing of $[(C_6H_6)RuCl(pmtca)]Cl$.

(TD-DFT) [7]. Calculations were performed with an all electron double-zeta-valence-polarized (DZVP) basis set [8], with *f* functions having exponents 1.94722036 and 0.748930908 on ruthenium (the core electrons on the Ru atom were replaced with an effective core potential (ECP)), and polarization functions for all other atoms: 6-31g(2d,p) – chlorine, 6-31g** – carbon, nitrogen, and 6-31g(d,p) – hydrogen. The PCM solvent model was used in the Gaussian calculations with methanol as the solvent. GaussSum 2.2 [9] was used to calculate group contributions to the molecular orbitals and to prepare partial density-of-states (DOS) and overlap population density-of-states (OPDOS) spectra. The contribution of a group to a molecular orbital was calculated using Mulliken population analysis. PDOS and OPDOS spectra were created by convoluting the molecular orbital information with the Gaussian curves of unit height and FWHM of 0.3 eV.

2.4. *Crystal structure determination and refinement*

A yellow crystal of $[(C_6H_6)RuCl(pmtca)]Cl \cdot 3H_2O$ was mounted on a Xcalibur, Atlas, Gemini ultra Oxford Diffraction automatic diffractometer equipped with a CCD detector and used for data collection. X-ray intensity data were collected with graphite monochromated Mo-Kα radiation ($\lambda = 0.71073$ Å) at temperature 295.0(2) K with ω-scan mode. Ewald sphere reflections were collected up to $2\theta = 50.05^\circ$. The unit cell parameters were determined from least-squares refinement of the setting angles of 12,710 strongest reflections. Details concerning crystal data and refinement are given in table 1. During the data reduction, the decay correction coefficient was taken into account. Lorentz, polarization, and numerical absorption corrections were applied. The structure was solved by the Patterson method. All non-hydrogen atoms were refined anisotropically using full-matrix least-squares technique on F^2. All the hydrogens were found from difference Fourier synthesis after four cycles of anisotropic refinement, and refined as "riding" on the adjacent atom with individual isotropic temperature factor equal to 1.2 times the value of equivalent temperature factor of the parent atom, with geometry idealization after each cycle. Olex2 [10] was used for all the calculations. Atomic scattering factors were those incorporated in the computer programs.

3. Results and discussion

The half-sandwich complex was obtained by the reaction of $[(C_6H_6)RuCl_2]_2$ with 2-(2-pyridyl)-4-methylthiazole-5-carboxylic acid (pmtca) in methanol. The elemental analysis of the complex is in good agreement with its formulation. In the IR spectrum of the studied compound the ring C=C and C=N stretching bands of pmtca are present at 1697 and 1532 cm^{-1}, respectively. The carboxyl ν_{OH} is at 3479 cm^{-1}. Stretching modes of the aryl C–H are visible at 3296 and 3069 cm^{-1}; methyl group stretching mode has maximum at 3020 cm^{-1}. The asymmetric and symmetric ν_{COO} stretching bands are visible at 1631, 1251 cm^{-1} and at 1928 cm^{-1} the $\nu_{C=O}$ of carbonyl group is present. The frequencies of water molecules are at 3650 and 1600 cm^{-1}. The stretching frequency of Ru–N bond has maximum at 439 cm^{-1}. In the ^1H NMR spectrum of the complex protons of C_6H_6 appear as a singlet at 5.613 ppm.

Table 1. Crystal data and structure refinement details of $[(C_6H_6)RuCl(pmtca)]Cl \cdot 3H_2O$.

Empirical formula	$C_{16}H_{20}Cl_2N_2O_5RuS$
Formula weight	524.38
Temperature (K)	295.0(2)
Crystal system	Monoclinic
Space group	*P2(1)/c*
Unit cell dimensions (Å, °)	
a	7.3118(2)
b	26.4039(8)
c	10.6014(3)
β	101.818(3)
Volume (Å^3)	2003.31(10)
Z	4
Calculated density (mg m^{-3})	1.739
Absorption coefficient (mm^{-1})	1.183
F(000)	1056
Crystal dimensions (mm^3)	$0.32 \times 0.11 \times 0.04$
θ range for data collection (°)	3.39 to 25.05
Index ranges	$-8 \le h \le 8$ $-31 \le k \le 31$ $-12 \le l \le 12$
Reflections collected	18065
Independent reflections	3399 [$R_{(int)} = 0.0199$]
Data/restraints/parameters	3399/0/267
Goodness-of-fit on F^2	1.122
Final *R* indices [$I > 2\sigma(I)$]	$R_1 = 0.0327$ $wR_2 = 0.0711$
R indices (all data)	$R_1 = 0.0391$ $wR_2 = 0.0726$
Largest difference peak and hole	0.627 and −0.557

3.1. *Crystal structures*

The obtained complex crystallizes in the monoclinic space group *P2(1)/c*. The molecular structure of the compound is shown in figure 1. The complex adopts a distorted piano-stool geometry with ruthenium π-bonded to benzene with an average Ru–C distance of 2.187(4) Å (range 2.171(4)–2.202(4) Å) and the distance between ruthenium and the centroid of the benzene ring is 1.687 Å. The ruthenium is also directly coordinated to nitrogens of N-heterocyclic ligand with distances of 2.106(3) and 2.114(3) Å; the Ru–Cl bond length is 2.403(10) Å. Angles between nitrogen heteroaromatic ligand and chloride are close to those observed in ruthenium arene compounds [11].

3.2. *Geometry and electronic structure*

Geometries were optimized in a singlet state by the DFT method with the B3LYP functional.

From the data collected in table 2, most differences between experimental and calculated geometry are in the benzene ring. The largest differences were found for the ruthenium–benzene carbon distances. The calculated Ru–benzene centroid distance is 1.763 Å. The natural atomic orbital d occupancies are: $d_{xy} = 1.77$, $d_{xz} = 1.66$, $d_{yz} = 1.66$, $d_{x^2y^2} = 0.78$, $d_{z^2} = 1.08$. This is a result of charge donation from ligands to ruthenium.

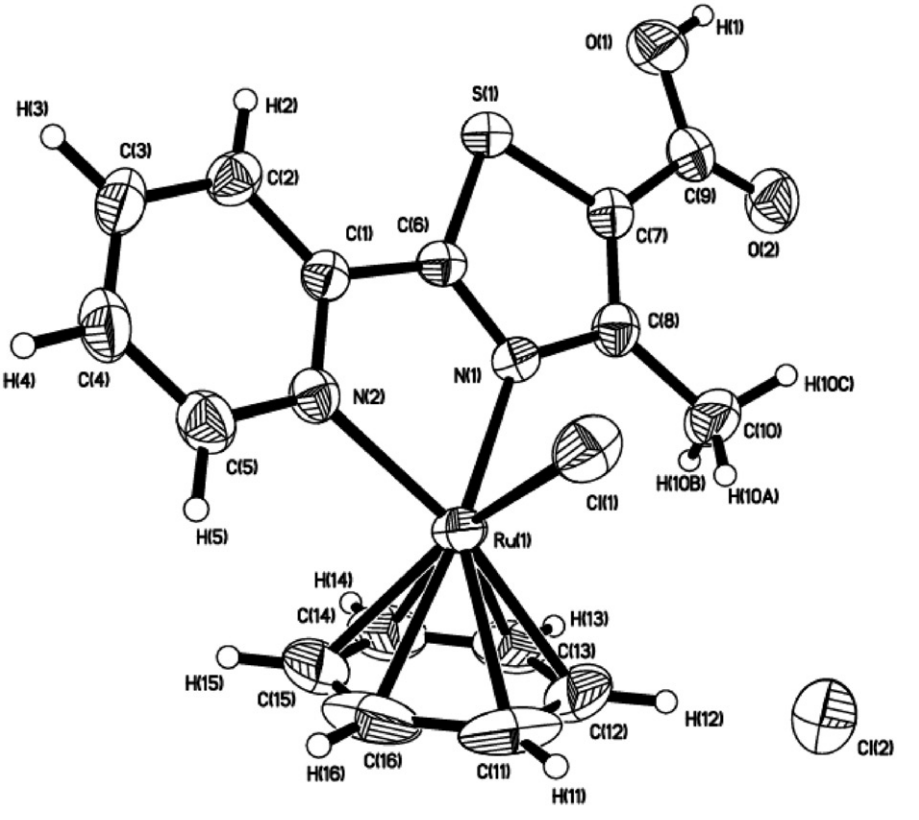

Figure 1. ORTEP of $[(C_6H_6)RuCl(pmtca)]Cl \cdot 3H_2O$ with 50% probability displacement ellipsoids. Water molecules are omitted for clarity.

The conclusion confirms the second-order perturbation analysis from NBO. The stabilization energy calculated in this analysis shows that the lone pairs localized on chloride and N-heteroaromatic ligand donate charge to ruthenium d orbitals and the stabilization energy (ΔE_{ij}) is 249.8 and 376.2 kcal mol^{-1}. The stabilization energy of the charge donation from benzene to antibonding d orbitals is about 604.6 kcal mol^{-1} and the back donation charge from ruthenium to benzene ring stabilized the molecule by 76.7 kcal mol^{-1} in $[(C_6H_6)RuCl(pmtca)]^+$. The stabilization energy associated with charge donation from ruthenium to N-donor ligand is 45.9 kcal mol^{-1}.

In the frontier region, neighboring orbitals are often closely spaced. In such cases, consideration of only the HOMO and LUMO may not yield a realistic description of the frontier orbitals. For this reason, DOS and OPDOS in terms of Mulliken population analysis were calculated using the GaussSum program. They provide a pictorial representation of molecular orbital compositions and their contributions to chemical bonding. The DOS and OPDOS diagrams are shown in figure 2. The DOS plot mainly presents the composition of the fragment orbitals contributing to the molecular orbitals. The OPDOS indicates bonding, nonbonding, and antibonding characteristics of the particular fragments. A positive value in OPDOS plots means a bonding interaction, while a negative value represents antibonding interaction and a value near zero indicates a nonbonding interaction.

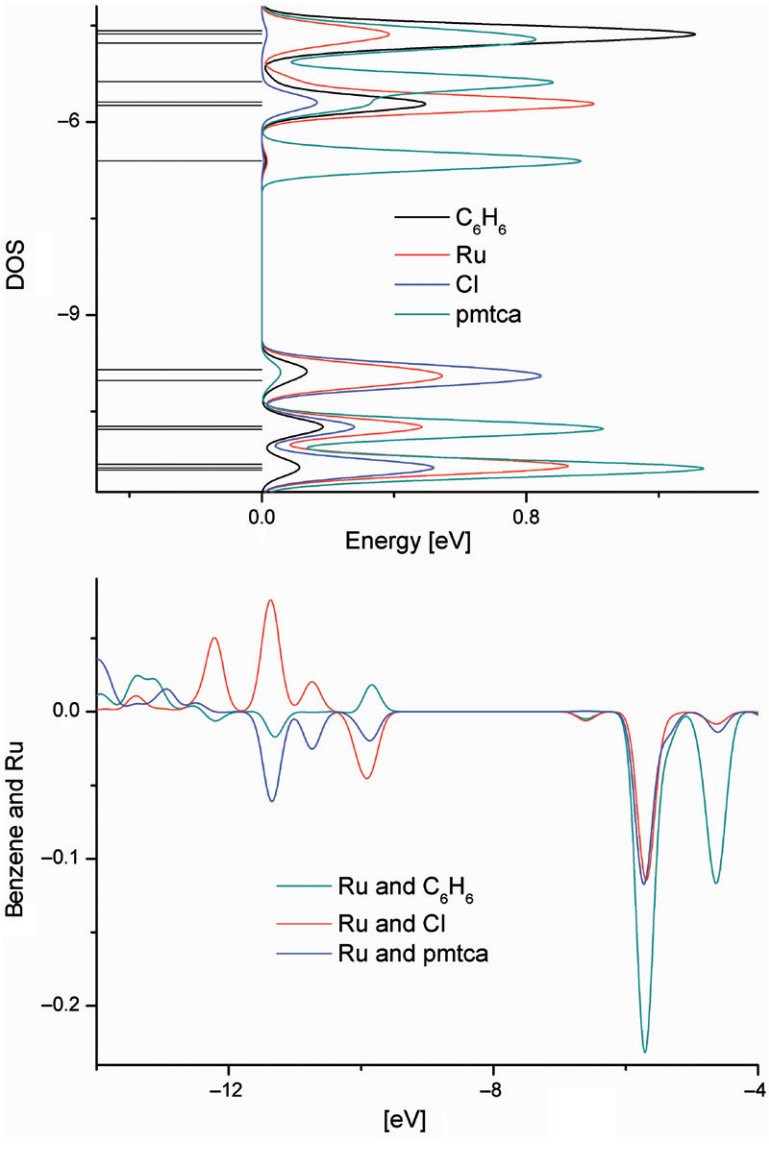

Figure 2. The DOS and OPDOS diagrams for $[(C_6H_6)RuCl(pmtca)]^+$.

As can be seen from the DOS diagram and the data in table 3 HOMO is mainly composed from ruthenium d (33%) and chlorine p (51%) orbitals and LUMO is localized on the 2-(2-pyridyl)-4-methylthiazole-5-carboxylic acid. The notable contribution of d ruthenium orbitals is visible in several HOMO up to HOMO–15, in the virtual molecular orbitals LUMO + 1, LUMO + 2, LUMO + 5, LUMO + 6, and LUMO + 9 have considerable contribution of d_{Ru} orbitals. This diffusion of ruthenium d orbitals is better visible on the DOS plot in figure 2. On the OPDOS graph are plotted the interactions of ruthenium with benzene, chloride, and pmtca. The interactions of benzene with Ru(II) d orbitals have positive values in the energy

Table 2. Selected bond lengths (Å) and angles (°) for $[(C_6H_6)RuCl(pmtca)]^+$ with optimized geometry values.

	Exp	Calcd
Ru(1)–N(1)	2.114(3)	2.1523
Ru(1)–N(2)	2.106(3)	2.1380
Ru(1)–Cl(1)	2.403(10)	2.3924
Ru(1)–C(11)	2.173(4)	2.2550
Ru(1)–C(12)	2.202(4)	2.2718
Ru(1)–C(13)	2.199(4)	2.2563
Ru(1)–C(14)	2.201(4)	2.2942
Ru(1)–C(15)	2.171(4)	2.2470
Ru(1)–C(16)	2.175(4)	2.2522
N(1)–Ru(1)–N(2)	76.57(10)	76.48
N(1)–Ru(1)–Cl(1)	84.39(7)	83.85
N(2)–Ru(1)–Cl(1)	85.17(8)	84.66
N(1)–Ru(1)–C(11)	148.15(19)	143.07
N(1)–Ru(1)–C(13)	95.83(14)	96.10
N(1)–Ru(1)–C(15)	131.11(19)	137.70
N(2)–Ru(1)–C(11)	133.72(18)	134.04
N(2)–Ru(1)–C(13)	141.97(16)	143.83
N(2)–Ru(1)–C(15)	91.03(15)	93.44
Cl(1)–Ru(1)–C(11)	88.42(13)	87.78
Cl(1)–Ru(1)–C(13)	131.75(14)	131.16
Cl(1)–Ru(1)–C(15)	142.28(18)	140.38
C(11)–Ru(1)–C(13)	66.59(18)	65.79
C(11)–Ru(1)–C(15)	67.6(2)	65.54
C(13)–Ru(1)–C(15)	65.80(19)	65.84

range adequate to HOMO and at lower HOMO the interactions have nonbonding and antibonding character. In highest HOMO orbitals chlorine and pmtca have antibonding interaction with metal ion. In the frontier occupied and virtual molecular orbital values of the interaction between ruthenium and 2-(2-pyridyl)-4-methylthiazole-5-carboxylic acid is small, which indicate the ligand as a weak π-acceptor. This conclusion is confirmed by the earlier mentioned stabilization energy (donation form ruthenium to pmtca) and by the proportion of Ru(II) and pmtca in frontier molecular orbitals and Mayer bond orders: Ru–Cl 2.07, Ru–N 0.79 and 0.84, Ru–C_6H_6 0.76 (average value).

Energy decomposition analysis based on the work of Morokuma [12] and the extended transition state (ETS) partitioning scheme of Ziegler [13] has been carried out using ADF program (Release 2008) [14] at the level of B3LYP/TZP [15]. The binding energy of the compound was calculated as the difference between the energy of the complex with the optimized geometry and the energies of the optimized ligands pmtca or benzene and fragments $[(C_6H_6)RuCl]^+$ or $[(pmtca)RuCl]^+$, respectively. General theoretical background on the bond energy decomposition scheme can be found in a review [16]. In table 4, the results of energy decomposition analysis calculated for the complex in gas phase and more realistic in methanol are listed. The Coulomb (steric and orbital interaction) energy plays an important role for $[(C_6H_6)RuCl]$-pmtca binding in solution. Additionally, the calculated binding energy is slightly more than the energy calculated toward the bonding of benzene with $[(pmtca)RuCl]^+$.

Table 3. Relative percentages of atomic and ligand molecules contributions to the lowest unoccupied and highest occupied molecular orbitals.

	Energy (eV)	C_6H_6	Ru	Cl	pmtca
L + 9	−2.57	29	64	0	8
L + 8	−3.48	0	2	0	97
L + 7	−3.77	1	2	0	97
L + 6	−4.58	51	15	1	34
L + 5	−4.63	68	20	1	12
L + 4	−4.77	30	9	0	60
L + 3	−5.37	3	9	0	87
L + 2	−5.69	24	53	16	8
L + 1	−5.74	26	49	1	23
LUMO	−6.6	1	2	1	96
HOMO	−9.85	12	33	51	5
H − 1	−10.02	4	36	57	2
H − 2	−10.73	16	41	23	21
H − 3	−10.78	3	8	6	83
H − 4	−11.32	4	59	17	19
H − 5	−11.38	4	19	17	60
H − 6	−11.41	4	19	19	58
H − 7	−12.21	8	29	53	10
H − 8	−12.33	1	3	6	90
H − 9	−12.49	10	4	3	83
H − 10	−12.56	7	1	1	91
H − 11	−12.92	12	8	1	79
H − 12	−13.11	42	15	0	42
H − 13	−13.41	46	19	8	28
H − 14	−13.85	19	14	1	66
H − 15	−13.98	17	12	0	71
H − 16	−14.11	14	8	0	78
H − 17	−14.5	90	1	0	9

Table 4. Energy decomposition analysis for $[(C_6H_6)RuCl(pmtca)]^+$ in the $[(C_6H_6)RuCl]$ fragment, pmtca and $[RuCl(pmtca)]^+$, and C_6H_6 fragments (energies in kcal mol^{-1}).

	$[(C_6H_6)RuCl]^+$ and pmtca		$[RuCl(pmtca)]^+$ and C_6H_6	
Energy (kcal mol^{-1})	Gas phase	CH_3OH solvent	Gas phase	CH_3OH solvent
ΔE_{elstat}	−176.88	−176.88	−212.96	−212.96
$\Delta E_{kinetic}$	−401.16	−464.81	−262.21	−322.19
$\Delta E_{Coulomb\ (Steric+OrbInt)}$	525.34	597.51	524.77	593.98
ΔE_{XC}	−50.14	−53.71	−138.14	−142.58
$\Delta E_{solvation}$		−65.43		−65.28
ΔE	−102.83	−163.32	−88.53	−149.03

3.3. *Electronic spectrum*

The UV-Vis spectra of the complexes displayed bands with maxima at 440 ($\log \varepsilon = 2.86$), 342 ($\log \varepsilon = 3.98$) shoulder, 329 ($\log \varepsilon = 4.15$) and 216 ($\log \varepsilon = 4.38$) nm. The longest wavelength experimental band was calculated for the transitions from HOMO and HOMO − 1 to LUMO (72%), LUMO + 1 (53%), and LUMO + 2 (72%). In this manner this transition has ligand field character ($d \rightarrow d$) with admixture of metal–ligand charge transfer ($d \rightarrow \pi^*_{pmtca}$). The shoulder of the next band arises from

transition between HOMO − 1 → LUMO (83%) and HOMO − 3 → LUMO (84%) and HOMO − 3 → LUMO + 1 (62%) and its character is the same as the previous band. In the energy range around 329 nm, the transitions between HOMO−2 → LUMO (83%) and HOMO → LUMO + 3 (85%) were calculated, which indicated that the band has MLCT character ($d \rightarrow \pi^*_{pmtca}$). The calculated transitions attributed to experimental one at 216 nm (HOMO − 7 → LUMO (69%), HOMO − 9 → LUMO (67%), HOMO − 3 → LUMO + 4 (61%), HOMO − 4 → LUMO + 3 (82%), HOMO − 5 → LUMO + 4 (72%)) are *ligand–ligand charge transfer* type ($\pi \rightarrow \pi^*$).

4. Conclusion

Summarizing, the new half-sandwich ruthenium(II) complex with 2-(2-pyridyl)-4-methylthiazole-5-carboxylic acid is synthesized. The molecular structure of the compound is determined by X-ray and the spectroscopic properties as IR and ^{1}H NMR spectra were studied. Based on the crystal structure, computational research was made to determine the electronic structure of the studied compound. Electronic structure was calculated using the DFT method. Apart from the descriptions of frontier molecular orbitals and the relocation of the electron density of the compounds, the bonding in the complex was also determined. Based on the calculated stabilization energies, the value of the interaction between ruthenium and N,S-heteroaromatic ligand and the energy decomposition analysis indicated that the ligand was rather a weak π-acceptor. The analysis of the frontier orbitals and the TD-DFT calculations were used to determine the electronic spectrum of $[(C_6H_6)RuCl(pmtca)]Cl \cdot 3H_2O$.

Supplementary material

CCDC 757910 contains the supplementary crystallographic data for the studied complex. The data can be obtained free of charge from http://www.ccdc.cam.ac.uk/conts/retrieving.html, or from the Cambridge Crystallographic Data Centre, 12 Union Road, Cambridge CB2 1EZ, UK; Fax: (+44) 1223-336-033; or E-mail: deposit@ccdc.cam.ac.uk. Calculations have been carried out in Wroclaw Centre for Networking and Supercomputing (http://www.wcss.wroc.pl).

References

[1] J. Reedijk. In *Comprehensive Coordination Chemistry*, G. Wilkinson, R.D. Gillard, J.A. McCleverty (Eds), Vol. 2, p. 73, Pergamon Press, Oxford (1987); K. Kalyansundaram, M. Grätzel. *Coord. Chem. Rev.*, **177**, 347 (1998); M.D. Ward. *Chem. Soc. Rev.*, **24**, 121(1995); W.T. Wong. *Coord. Chem. Rev.*, **131**, 45 (1994); V. Balzani, A. Credi, F. Scandola. In *Transition Metals in Supramolecular Chemistry*, L. Fabbrizzi, A. Poggi (Eds), p. 1, Kluwer, Dordrecht, The Netherlands (1994); A. Anderson, R.F. Anderson, M. Furue, P.C. Junk, R.F. Keene, B.T. Patterson, B.D. Yeomens. *Inorg. Chem.*, **39**, 2721 (2000); A.H. Velders, A.G. Quiroga, J.G. Haasnoot, J. Reedijk. *Eur. J. Inorg. Chem.*, 713 (2003), and references therein.

[2] M.A. Bennett. In *Comprehensive Organometallic Chemistry II*, E.W. Abel, F.G.A. Stone, G. Wilkinson (Eds), Vol. 7, Pergamon Press, Oxford (1995).

[3] A. Schlüter, K. Bieber, W.S. Sheldrick. *Inorg. Chim. Acta*, **340**, 35 (2002); Y. Chen, M. Valentini, P.S. Pregosin, A. Albinati. *Inorg. Chim. Acta*, **327**, 4 (2002); A. Singh, N. Singh, D.S. Pandey. *J. Organomet. Chem.*, **642**, 48 (2002); R. Lalrempuia, H.P. Yennawar, M.R. Kollipara. *J. Coord. Chem.*, **62**, 3661 (2009).
[4] M.A. Bennett, T.-N. Huang, T.W. Matheson, A.K. Smith. *Inorg. Synth.*, **21**, 74 (1982).
[5] M.J. Frisch, G.W. Trucks, H.B. Schlegel, G.E. Scuseria, M.A. Robb, J.R. Cheeseman, G. Scalmani, V. Barone, B. Mennucci, G.A. Petersson, H. Nakatsuji, M. Caricato, X. Li, H.P. Hratchian, A.F. Izmaylov, J. Bloino, G. Zheng, J.L. Sonnenberg, M. Hada, M. Ehara, K. Toyota, R. Fukuda, J. Hasegawa, M. Ishida, T. Nakajima, Y. Honda, O. Kitao, H. Nakai, T. Vreven, J.A. Montgomery Jr, J.E. Peralta, F. Ogliaro, M. Bearpark, J.J. Heyd, E. Brothers, K.N. Kudin, V.N. Staroverov, R. Kobayashi, J. Normand, K. Raghavachari, A. Rendell, J.C. Burant, S.S. Iyengar, J. Tomasi, M. Cossi, N. Rega, J.M. Millam, M. Klene, J.E. Knox, J.B. Cross, V. Bakken, C. Adamo, J. Jaramillo, R. Gomperts, R.E. Stratmann, O. Yazyev, A.J. Austin, R. Cammi, C. Pomelli, J.W. Ochterski, R.L. Martin, K. Morokuma, V.G. Zakrzewski, G.A. Voth, P. Salvador, J.J. Dannenberg, S. Dapprich, A.D. Daniels, O. Farkas, J.B. Foresman, J.V. Ortiz, J. Cioslowski, D.J. Fox. *Gaussian 09*, Revision A.1, Gaussian, Inc., Wallingford, CT (2009).
[6] A.D. Becke. *J. Chem. Phys.*, 98, 5648 (1993); C. Lee, W. Yang, R.G. Parr. *Phys. Rev. B*, 37, 785 (1988).
[7] M.E. Casida. In *Recent Developments and Applications of Modern Density Functional Theory, Theoretical and Computational Chemistry*, J.M. Seminario (Ed.), Vol. 4, p. 391, Elsevier, Amsterdam (1996).
[8] K. Eichkorn, F. Weigend, O. Treutler, R. Ahlrichs. *Theor. Chim. Acc.*, **97**, 119 (1997).
[9] N.M. O'Boyle, A.L. Tenderholt, K.M. Langner. *J. Comp. Chem.*, **29**, 839 (2008).
[10] O.V. Dolomanov, L.J. Bourhis, R.J. Gildea, J.A.K. Howard, H. Puschmann. *J. Appl. Cryst.*, **42**, 339 (2009).
[11] R. Tribo, J. Pons, R. Yanez, J.F. Piniella, A. Alvarez-Larena, J. Ros. *Inorg. Chem. Commun.*, **3**, 545 (2000); M. Jahncke, A. Neels, H. Stoeckli-Evans, G. Süss-Fink. *J. Organomet. Chem.*, **561**, 227 (1998); H. Kurosawa, H. Asano, Y. Miyaki. *Inorg. Chim. Acta*, **270**, 87 (1998).
[12] K.J. Morokuma. *Chem. Phys.*, **55**, 1236 (1971).
[13] T. Ziegler, A. Rauk. *Theor. Chim. Acta*, **46**, 1 (1977).
[14] ADF2009.01, SCM, Theoretical Chemistry, Vrije Universiteit, Amsterdam, The Netherlands, http://www.scm.com
[15] P.J. Stephens, F.J. Devlin, C.F. Chablowski, M.J. Frisch. *J. Phys. Chem.*, **98**, 11623 (1994).
[16] F.M. Bickelhaupt, E.J. Baerends. In *Reviews in Computational Chemistry*, K.B. Lipkowitz, D.B. Boyd (Eds), Vol. 15, pp. 1–86, Wiley-VCH, New York (2000).